JOURNAL OF GEOPHYSICAL RESEARCH, VOL. 113, B09213, doi:10.1029/2007JB005229, 2008

Experimental determination of the elasticity of iron at high pressure

Wendy L. Mao,[1] Viktor V. Struzhkin,[2] Alfred Q. R. Baron,[3,4] Satoshi Tsutsui,[4] Caterina E. Tommaseo,[5] Hans-Rudolf Wenk,[6] Michael Y. Hu,[7] Paul Chow,[7] Wolfgang Sturhahn,[8] Jinfu Shu,[2] Russell J. Hemley,[2] Dion L. Heinz,[9] and Ho-Kwang Mao[2,7]

Received 14 June 2007; revised 11 March 2008; accepted 26 June 2008; published 30 September 2008.

[1] We present a multitechnique approach to experimentally determine the elastic anisotropy of polycrystalline hcp Fe at high pressure. Directional phonon measurements from inelastic X-ray scattering on a sample with lattice preferred orientation at 52 GPa in a diamond anvil cell were coupled with X-ray diffraction data to determine the elastic tensor. Comparison of the results from this new method with the elasticity determined by lattice strain analysis of radial X-ray diffraction measurements showed significant differences, highlighting the importance of strength anisotropy in hcp Fe. At 52 GPa, we found that a method which combines results from inelastic scattering and pressure-volume measurements gives a shape in the velocity anisotropy close to sigmoidal (with a faster *c* and slower *a* axis) a smaller magnitude in the anisotropy and compared to velocities based on the lattice strain method which gives a bell shape velocity distribution with the fast direction between the *c* and *a* axes. We used additional results from nuclear resonant inelastic X-ray scattering to constrain errors and provide additional validation of the accuracy of our results.

Citation: Mao, W. L., et al. (2008), Experimental determination of the elasticity of iron at high pressure, *J. Geophys. Res.*, *113*, B09213, doi:10.1029/2007JB005229.

1. Introduction

[2] Located over 5000 km below the Earth's surface, the inner core represents the most remote region within the planet. Seismology has provided a wealth of information on the elastic behavior of this region in the Earth. It has been established that the inner core exhibits elastic anisotropy with compressional waves traveling approximately 3% faster in the polar versus equatorial direction [e.g., *Creager*, 1992; *Morelli et al.*, 1986; *Shearer*, 1994; *Song and Helmberger*, 1993; *Tromp*, 1993; *Woodhouse et al.*, 1986]. There may also be additional complications in the structure within the inner core such as variations in anisotropy with depth and hemispherical differences [e.g., *Bréger et al.*, 2000; *Cao and Romanowicz*, 2004; *Creager*, 1999; *Ishii and Dziewonski*, 2002; *Romanowicz et al.*, 2002; *Song and Helmberger*, 1995; *Sun and Song*, 2002; *Vinnik et al.*, 1994]. Since the Earth's inner core is predominantly composed of Fe [*Birch*, 1952] and existing data indicate that hexagonal close packed (hcp) Fe is the stable phase at inner core conditions [e.g., *Ma et al.*, 2004; *Mao et al.*, 1990; *Stixrude et al.*, 1997; *Vocadlo et al.*, 2000; *Hemley and Mao*, 2001], determination of elastic and other physical properties of hcp Fe at high pressure and temperature (*P-T*) is crucial for understanding this portion of the planet.

[3] Key elasticity and texture properties to be determined include the compressibility of the unit cell parameters, bulk and shear moduli (K and G), aggregate compressional and shear wave velocities (V_P and V_S), single-crystal elastic tensor (C_{ij} or S_{ij}), single-crystal V_P and V_S as a function of crystallographic orientation (ψ), lattice preferred orientation (LPO) under axial stress, and shear strength (t). During the last decade, an impressive number of high-pressure techniques have become available for measuring these properties in the diamond anvil cell (DAC) to core pressures, and some properties can now be measured by several independent techniques, each with its own merits and limitations. Elastic parameters obtained from a single technique often require assumptions and extrapolations that can lead to contradictory conclusions. Integration of complementary experimental techniques has potential for providing an optimized, robust answer if they are strategically combined. Here we review the strengths, weaknesses, and

[1]Department of Geological and Environmental Sciences and Photon Science, SLAC, Stanford University, Stanford, California, USA.
[2]Geophysical Laboratory, Carnegie Institution of Washington, Washington, D.C., USA.
[3]SPring-8, RIKEN, Sayo, Japan.
[4]SPring-8, JASRI, Sayo, Japan.
[5]Department of Crystallography, University of Göttingen, Göttingen, Germany.
[6]Department of Earth and Planetary Science, University of California, Berkeley, California, USA.
[7]HPCAT, Advanced Photon Source, Carnegie Institution of Washington, Washington, D.C., USA.
[8]XOR, Advanced Photon Source, Argonne National Laboratory, Argonne, Illinois, USA.
[9]Department of Geophysical Sciences, University of Chicago, Chicago, Illinois, USA.

0148-0227/08/2007JB005229$09.00

complementarities of individual techniques, and present an integrated approach (i.e., applying different techniques to make measurements on the same sample and utilizing their individual strengths to derive a complete, self-consistent set of elastic parameters) for studying hcp Fe, and demonstrate this approach with a comprehensive experiment at 52 GPa.

2. Elasticity and Deformation of Iron at High Pressures

2.1. Seismic Observations and Aggregate Sound Velocities

[4] Measurements of V_P, V_S, and the seismic parameter (Φ) determined for regions within the Earth by seismology are related to materials properties by

$$\Phi = \frac{K_S}{\rho} = V_P^2 - \frac{4}{3}V_S^2, \frac{G}{\rho} = V_S^2 \quad (1)$$

For comparison to experiment, the values for the unit cell parameters, density (ρ), and adiabatic bulk modulus(K_S) can be determined from the isothermal equation of state (EOS) measured by X-ray diffraction (XRD) [*Dewaele et al.*, 2006; *Jephcoat et al.*, 1986] Differentiation of the P-ρ EOS yields the isothermal bulk modulus, K_T, which is related to K_S by

$$K_S = (1 + \alpha\gamma T)K_T \quad (2)$$

where the product of thermal expansivity (α) and Grüneisen parameter (γ) and T at low temperature is a small number that can be measured or estimated without introducing significant error to K_S. To fully calculate G, V_P, and V_S, nuclear resonant inelastic X-ray scattering (NRIXS) can be used to determine the Debye velocity (V_D) [*Hu et al.*, 2003] which gives the second equation in addition to equation (1) for calculating V_P and V_S:

$$\frac{3}{V_D^3} = \frac{1}{V_P^3} + \frac{2}{V_S^3} \quad (3)$$

NRIXS is particularly useful for constraining V_s and G that are difficult to obtain for high-pressure hcp Fe from other techniques. Other thermodynamic parameters (e.g., heat capacity, entropy, Debye temperature, and Grüneisen parameter) can be calculated from the integration of the phonon density of state (DOS) [*Mao et al.*, 2001]. Stable, in situ laser heating may also make high P-T NRIXS measurements that approach core conditions possible [*Lin et al.*, 2004].

2.2. Elastic Moduli and Sound Velocities

[5] Single crystals of hcp Fe cannot be synthesized at high P-T, precluding the experimental determination of the full phonon dispersion curves of hcp Fe which would provide the complete single crystal elastic tensor and the full information on elasticity and sound velocities. However, there are a number of experimental methods for determining sound velocities of polycrystalline hcp Fe at high pressure. Inelastic neutron scattering and ultrasonic measurements require large samples which limit the pressures that can be reached. The energy range for phonon dynamics is also accessible via optical methods each with its own advantages and limitations. Brillouin spectroscopy has long been used to study materials at high pressure and is a very powerful technique for measurement of V_P and V_S from the initial slope of the dispersion curve (see for example [*Bassett and Brody*, 1977; *Murakami et al.*, 2007; *Zha et al.*, 2000]). However, the range of the momentum transfer is close to zero as limited by the wavelengths of visible light, (i.e., $q = 4\pi \sin\theta/\lambda$, $q_{\max} \sim 0.02-0.03$ nm^{-1}) requiring samples to be transparent. Raman scattering generally probes optical (as opposed to acoustic) modes near the Brillouin zone center. In the case of hcp metals, however, the presence of a glide plane that bisects the unit cell along the c axis as indicated by the $P6_3/mmc$ space group, causes the dispersion curve to fold over at the Brillouin zone edge, thus doubling the reciprocal lattice in the c direction. This gives a dispersion curve maximum for an acoustic branch associated with the C_{44} shear elastic moduli at the zone center that can be probed by Raman spectroscopy for calculating vibrational properties [*Merkel et al.*, 2000; *Olijnyk and Jephcoat*, 2000; *Olijnyk et al.*, 2001]. Another technique using an optical wavelength probe is impulsive stimulated light scattering (ISLS) which has recently been applied for studying opaque samples like hcp Fe, giving data akin to ultrasonic measurements (i.e., both V_S and V_P) [*Crowhurst et al.*, 2004].

[6] Unlike optical measurements where clarity and parallelism are critical, inelastic X-ray scattering (IXS) utilizes X rays to probe the bulk sample and are not as sensitive to surface conditions. While these challenging, photon-intensive experiments are only feasible at 3rd generation synchrotron sources, they show great promise for studying elasticity to core pressures [*Fiquet et al.*, 2001]. Thus far, V_S has never been detected in IXS studies of hcp Fe, and the measurement is limited to V_P under uniaxial stress.

2.3. Strength and Lattice Preferred Orientation

[7] While the study by *Antonangeli et al.* [2004b] shows the possibility of using IXS to make directional phonon measurements on an axially compressed hcp Fe sample by probing at different angles relative to the DAC compression axis, multiple points over the full angular range are needed to constrain the shape of the velocity anisotropy. Indeed all previous experimental studies of sound velocities for hcp Fe at high pressure suffer from lack of characterization of the LPO of the sample, having to assume, be it explicitly or implicitly, a particular preferred orientation pattern of the sample (e.g., random texture versus complete alignment of c axis with the compressional axis). DAC experiments at ambient temperature indicate that hcp Fe crystals display strong preferred orientation, with c axes aligned parallel to the compression direction [*Merkel et al.*, 2000; *Wenk et al.*, 2000]. The degree of alignment depends on a number of factors (e.g., P-T conditions, strain and strain history, gasket material). Without measuring the LPO and the elasticity of the same sample at the same conditions it may be inappropriate to compare results from different techniques where experimental history could affect the LPO that develops in the sample.

[8] Radial X-ray diffraction (RXD) allows characterization of the LPO of a sample under axial stress through analysis of the intensity variations around Debye-Scherrer

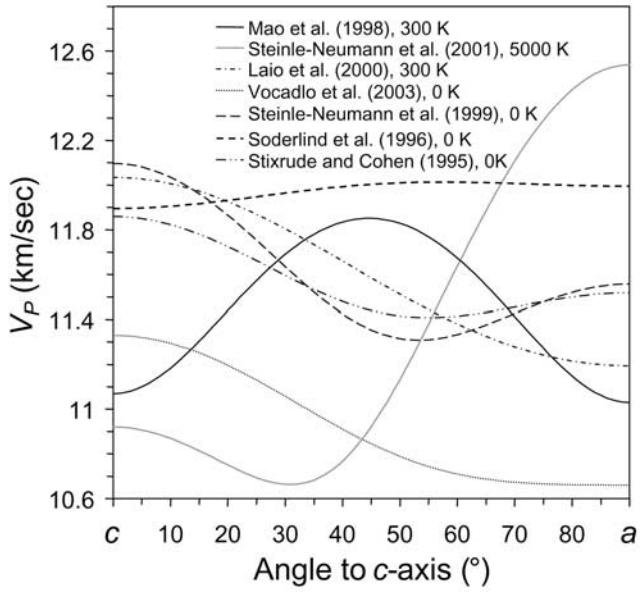

Figure 1. Comparison of compressional sound velocity (V_P) as a function of angle to c axis for different studies at 200 GPa. RXD-elasticity measurement is solid black line [*Mao et al.*, 1998]; 5000 K calculation is solid gray line [*Steinle-Neumann et al.*, 2001]; 300 K calculation is dash-dotted line [*Laio et al.*, 2000]; 0 K calculations are dotted line [*Vocadlo et al.*, 2003]; dashed line [*Steinle-Neumann et al.*, 1999]; long dashed line [*Söderlind et al.*, 1996]; and dash-dot-dotted line [*Stixrude and Cohen*, 1995]. After *Antonangeli et al.* [2004b] with permission from Elsevier.

rings from different reflections which can then be used to calculate the orientation distribution [*Wenk et al.*, 2006]. We will refer to this method as RXD-LPO. RXD also provides an alternative means of determining single crystal elastic moduli from lattice strain analysis [*Singh et al.*, 1998a, 1998b] which we will refer to as RXD-elasticity, but calculations of the elastic tensor include assumptions which could potentially introduce significant errors [*Mao et al.*, 1998]. Results from this technique need to be confirmed and corrected using results from other experimental measurements like directional phonon studies.

[9] An ambient temperature RXD-elasticity study on polycrystalline hcp Fe to 30 GPa demonstrated progress in constraining uncertainties when using this technique for determining single crystal elasticity [*Merkel et al.*, 2005]. Besides improvements that come with using large area detectors which enable precise measurements of the variation of d spacing with orientation, the inversion of elastic moduli was more sophisticated, including effects of LPO in the analysis [*Matthies et al.*, 2001], and using the constraint of the C_{44} elastic modulus measured using Raman spectroscopy [*Merkel et al.*, 2000]. For this lower pressure study, the overall shape of the anisotropy that was obtained was similar to that in previous work by [*Mao et al.*, 1998] (i.e., bell shape with fast body diagonal and slower a and c axes), but the magnitude was significantly reduced. A recent study of hcp Co, an analog material to hcp Fe, demonstrated that the orientation dependence of differential stress resulting from plastic deformation can be potential source of error in RXD-elasticity calculations [*Merkel et al.*, 2006]. The RXD-elasticity results for polycrystalline hcp Co did not reproduce the anisotropy shape determined by IXS measurements on single-crystal hcp Co which found a sigmoidal shape with a fast c and slow a axis [*Antonangeli et al.*, 2004a].

2.4. Theoretical Studies

[10] Theory is also a very powerful method for determining the properties of materials at high P-T. A number of first principles molecular dynamics studies have reported elastic properties for hcp Fe with differing results. The first principles calculations of *Stixrude and Cohen* [1995] found hcp Fe to be elastically anisotropic with a fast c axis and slower body diagonal and a axis. In order to explain seismic observations, the inner core would need to consist of perfectly aligned hcp Fe crystals with elastic properties equivalent to a single crystal. *Söderlind et al.* [1996] in contrast determined that the fast direction was oblique to the c axis, and propagation along the a axis was faster than the c axis. *Steinle-Neumann et al.* [1999] calculated results similar to the earlier *Stixrude and Cohen* [1995] result but found higher anisotropy. *Laio et al.* [2000], using an approach that combined first principles with classical molecular dynamics, also found a fast $c$and slow a axis, and more recently, *Vocadlo et al.* [2003] reported a similar result. All these calculations were for low temperature and thus are not directly applicable to anisotropy in the inner core. Thermal effects were considered by *Steinle-Neumann et al.* [2001], who concluded that the longitudinal anisotropy reverses at high temperature, with a fast crystallographic a direction relative to the c direction. However, this conclusion has not been supported by more recent theoretical [*Gannarelli et al.*, 2005] and experimental [*Ma et al.*, 2004] results. The strength of calculations is that they can cover the entire P-T range of the inner core, but contradictory results highlight the need for experimental verification of theory over the P-T region accessible in the laboratory.

[11] Despite the flurry of experimental and theoretical studies in the past decade a consensus has not been reached on the elasticity of hcp Fe; results from various studies often lead to contradictory conclusions for Earth core models. Figure 1 illustrates these dramatic differences at 200 GPa. RXD-elasticity results show the V_P maximum at 45° to the c axis of hcp Fe and minima at the c (0°) and a axes (90°) [*Mao et al.*, 1998], while as mentioned previously, the theoretical calculations show a range of results. The aggregate V_P and V_S obtained from different theoretical and experimental techniques also differ. As a result, *Fiquet et al.* [2001] used IXS results on hcp Fe to conclude that the inner core is lighter than pure Fe, while *Mao et al.* [2001] used NRIXS data to conclude that the inner core is heavier than pure Fe.

3. Experimental Procedures

3.1. Using an Integrated Set of Probes on the Same Sample

[12] In this study, we aim to establish an accurate method for determination of elastic anisotropy of hcp Fe at high pressure. We applied complementary experimental techni-

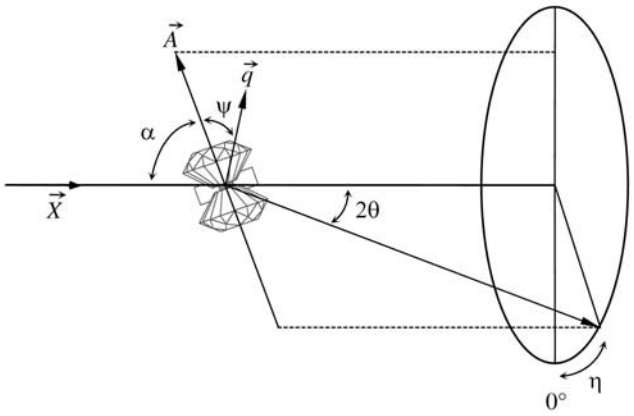

Figure 2. Radial diffraction scattering geometry. The parameter 2θ is the diffraction angle; η is the azimuth angle; ψ is the angle between the diamond compression axis and the momentum transfer; and α is the angle between the diamond compression axis and the incoming X ray. The angle of tilt, α, is about 20° away from 90° to avoid scattering of the Be gasket by the direct X-ray beam.

ques on the same sample at the same conditions in order to establish a benchmark data point at 52 GPa and ambient temperature. We were able to get nearly equivalent information from polycrystalline samples as we would from a single crystal via the combination of RXD-LPO, IXS directional phonon, and EOS measurements. We then used NRIXS to provide additional experimental constraints on our results and as a confirmation and redundancy check. We compared our results with those using RXD-elasticity. The merits and weaknesses of each technique are assessed and the results are integrated to determine hcp Fe elasticity at 52 GPa. The results also provide future direction for developing an optimized approach for studying elasticity at higher P and T than explored in our experiments.

[13] A panoramic DAC which is compatible with all these probes was used in the present study. The Fe powder (submicron grain size) sample was loaded into a 150 μm sample chamber in a Be gasket and compressed between flat diamonds with 500 μm culets. The average pressure in the sample was determined from the hcp Fe volume measured using RXD as discussed in section 3.2. No pressure-transmitting medium was added in order to generate the nonhydrostatic stress necessary for the development of lattice preferred orientation.

3.2. Lattice Strain Under Axial Compression

[14] Angle-dispersive RXD was conducted at beam line 16-IDB (HPCAT) of the Advanced Photon Sources (APS), Argonne National Laboratory (ANL). A monochromatic X-ray beam (λ = 0.3678 Å, beam size ~16 × 17 μm) was focused using Kirkpatrick-Baez mirrors through the gasket onto the polycrystalline Fe sample that was subjected to axial stress in the DAC in the scattering geometry shown in Figure 2. The DAC was tilted by $\alpha = 17°$ in order to reduce the diffraction from the beryllium gasket. RXD allows access to small d spacing (large 2θ) reflections that are normally cutoff by the X-ray absorbing seats in axial diffraction experiments. A CeO_2 standard was used to calibrate the detector distance and tilt, and the RXD patterns were collected using a MAR3450 image plate detector.

[15] We observed eight hcp Fe reflections, 100, 002, 101, 102, 110, 103, 112, and 201 (Figure 3), and determined d spacings of each hkl as a function of η (Figure 4). Azimuth angle, η is related to ψ by the following relation:

$$\cos\psi = \cos\eta\cos\theta\sin\alpha - \sin\theta\cos\alpha \tag{4}$$

The diffraction profiles were integrated over 5° angular azimuthal slices from η = 0° to 360° [*Hammersley*, 1997]. For the smaller d spacing (large 2θ) lines, there was some limitation to the η access due to the detector size and sample to detector distance.

[16] The stress state of the specimen compressed between two anvils is a superposition of the hydrostatic (σ_P) and deviatoric (d_{ij}) stress components. The deviatoric strain (relative to the hydrostatic strain) produced by d_{ij} at a particular crystallographic orientation, ψ is given by

$$\varepsilon_\psi(hkl) = \frac{\left[d_\psi(hkl) - d_P(hkl)\right]}{d_P(hkl)} \tag{5}$$

the difference between the d spacing measured at ψ, $d_\psi(hkl)$, and the d spacing under hydrostatic pressure σ_P, $d_P(hkl)$. The average pressure in the sample was determined from the Fe EOS by using $d_P(hkl)$ to calculate the volume [*Jephcoat et al.*, 1986] and was found to be 52 GPa for this sample. For elastically isotropic materials, the strain is identical for all hkl, but for elastically anisotropic materials, ε_ψ varies with hkl. The dependence of ε_ψ on hkl contains a wealth of information related to the elastic moduli (C_{ij}) and/or lattice strength anisotropy. Combined with additional information from a separate XRD study under hydrostatic compression, sufficient equations are obtained for solving the C_{ij} matrix. On the basis of anisotropic linear elasticity theory [*Singh et al.*, 1998a], the experimentally measured $\varepsilon_\psi(hkl)$ as a function of ψ has the form:

$$\varepsilon_\psi(hkl) = \left(1 - 3\cos^2\psi\right)\cdot Q(hkl) \tag{6}$$

Equation (6) is general and valid for all crystal systems. Plots of $\varepsilon_\psi(hkl)$ versus $1-3\cos^2\psi$ (Figure 5) can be used to compute $Q(hkl)$. Depending on the crystal class, $Q(hkl)$ is a function of hkl and a set of m_i; each m_i is an independent linear combination of S_{ij} (or C_{ij}). The set of m_i equations, combined with additional linear equations from the axial compressibilities, are used to calculate the S_{ij}. For a hexagonal system like hcp Fe,

$$Q(hkl)/t = m_1 + m_2 H + m_3 H^2 \tag{7}$$

where

$$H = \frac{3a^2l^2}{\left[4c^2(h^2+hk+k^2) + 3a^2l^2\right]} \tag{8}$$

$$m_1 = (2S_{11} - S_{12} - S_{13})/6 \tag{9}$$

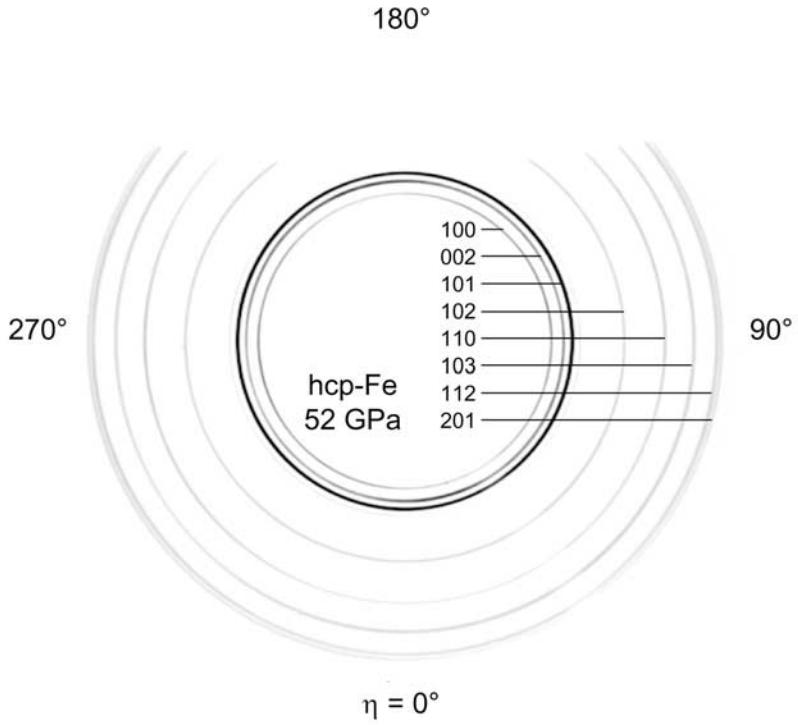

Figure 3. RXD image of hcp Fe at 52 GPa. The *hkl* reflections corresponding to the observed Debye-Scherrer rings are labeled. At $\eta = 0°$ and 180° the Debye-Scherrer rings shift to larger 2θ (smaller d spacing).

$$m_2 = (-5S_{11} + S_{12} + 5S_{13} - S_{33} + 3S_{44})/6 \quad (10)$$

$$m_3 = (S_{11} - 2S_{13} + S_{33} - S_{44})/2 \quad (11)$$

The three parameters, m_1, m_2, and m_3, of the quadratic equation (equation (7)) were determined experimentally by fitting a parabola to the $Q(hkl)/t$ versus H data, and provide three equations for S_{ij} (Figure 6). The hydrostatic linear compressibilities of the a and c axes are defined as $\chi_a = -(\partial a/\partial P)_S/a$ and $\chi_c = -(\partial c/\partial P)_S/c$. They are related to S_{ij} by:

$$\chi_a = S_{11} + S_{12} + S_{13} \quad (12)$$

$$\chi_c = S_{33} + 2S_{13} \quad (13)$$

which provide two additional equations for solving the five S_{ij} for the hexagonal crystal. Values for χ_a and χ_c were determined from the hydrostatic EOS of hcp Fe [*Jephcoat et al.*, 1986].

[17] In the above analysis, we introduced a new unknown, t. For the isostress condition, the t values are estimated using the relation,

$$t = 6G\langle Q\rangle \quad (14)$$

where G is the shear modulus of the bulk specimen at σ_p, and $\langle Q\rangle$ denotes the average value of $Q(hkl)$ for all observed reflections. The high-pressure value for G came from our hydrostatic NRIXS measurement (see section 3.5). The C_{ij}, for a hexagonal system, are related to the S_{ij} by the following simple relations:

$$C_{11} + C_{12} = S_{33}/S \quad (15)$$

$$C_{11} - C_{12} = 1/(S_{11} - S_{12}) \quad (16)$$

$$C_{13} = -S_{13}/S \quad (17)$$

$$C_{33} = (S_{11} + S_{12})/S \quad (18)$$

$$C_{44} = 1/S_{44} \quad (19)$$

$$S = S_{33}(S_{11} + S_{12}) - 2S_{13}^2 \quad (20)$$

The calculated values for the elastic tensor components are given in Table 1 and are in agreement with previous RXD-elasticity results [*Mao et al.*, 1998]. The acoustic velocities can then be calculated as a function of crystallographic direction from the elastic constants using the following relations for a hexagonal crystal [*Musgrave*, 1970; *Zha et al.*, 1993]. For the compressional wave,

$$\rho V_P^2 = \frac{A + B}{2} \quad (21)$$

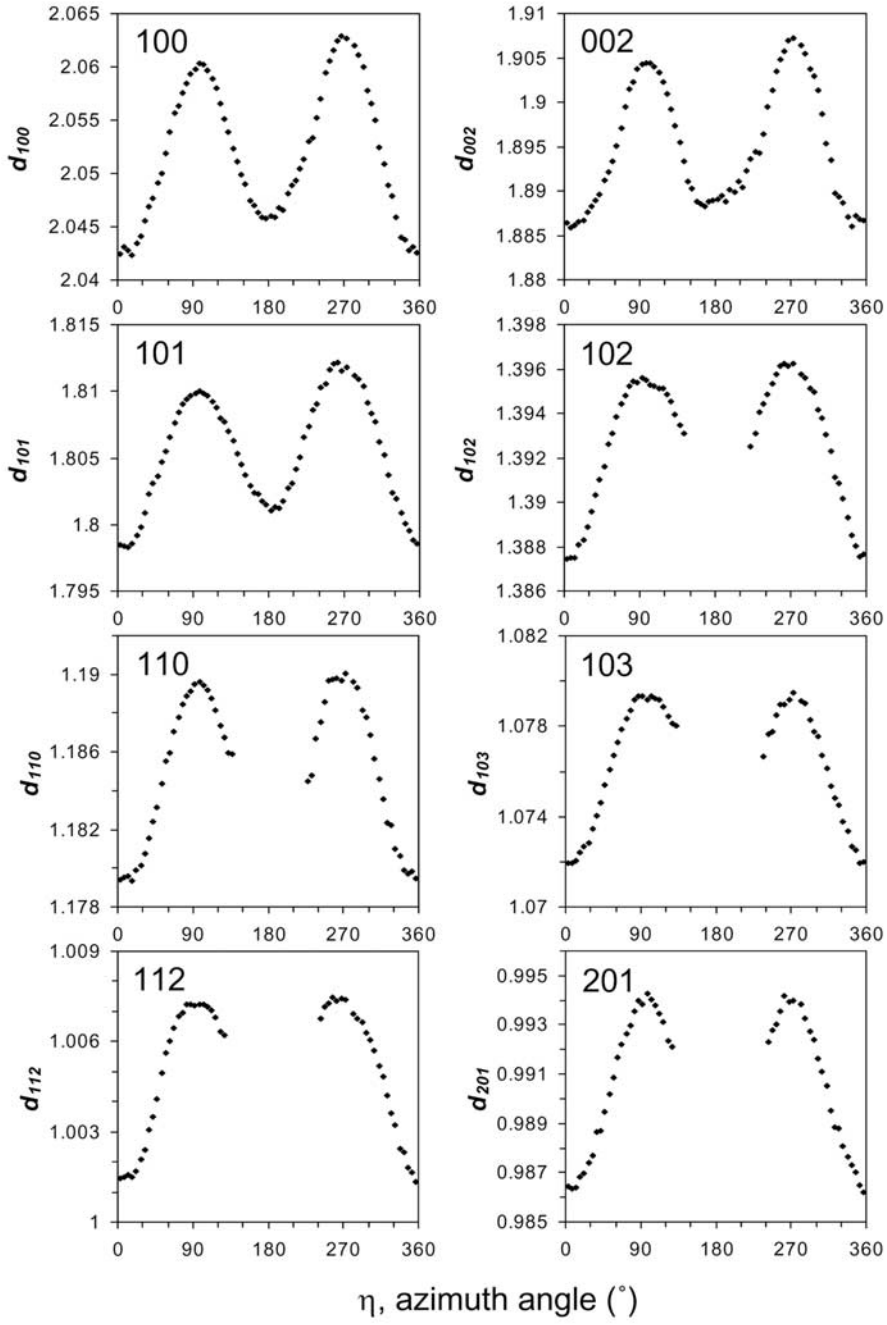

Figure 4. The d spacing as a function of azimuth angle (η) for different hcp Fe reflections. Over the interval from $\eta = 130°$ to $230°$ the lower d spacing (higher 2θ) reflections are cutoff because diffraction was blocked by the diamond anvil cell.

where A and B are given by:

$$A = C_{11}\sin^2\psi + C_{33}\cos^2\psi + C_{44} \tag{22}$$

$$B^2 = \left[(C_{11} - C_{44})\sin^2\psi + (C_{44} - C_{33})\cos^2\psi\right]^2 + (C_{13} + C_{44})^2\sin^2 2\psi \tag{23}$$

and ψ is the angle relative to the c axis (Figure 7). Note that for $\psi = 0°$,

$$\rho V_P^2(0°) = C_{33} \tag{24}$$

and taking advantage of the cylindrical symmetry for the hcp system, for $\psi = 90°$,

$$\rho V_P^2(90°) = C_{11} \tag{25}$$

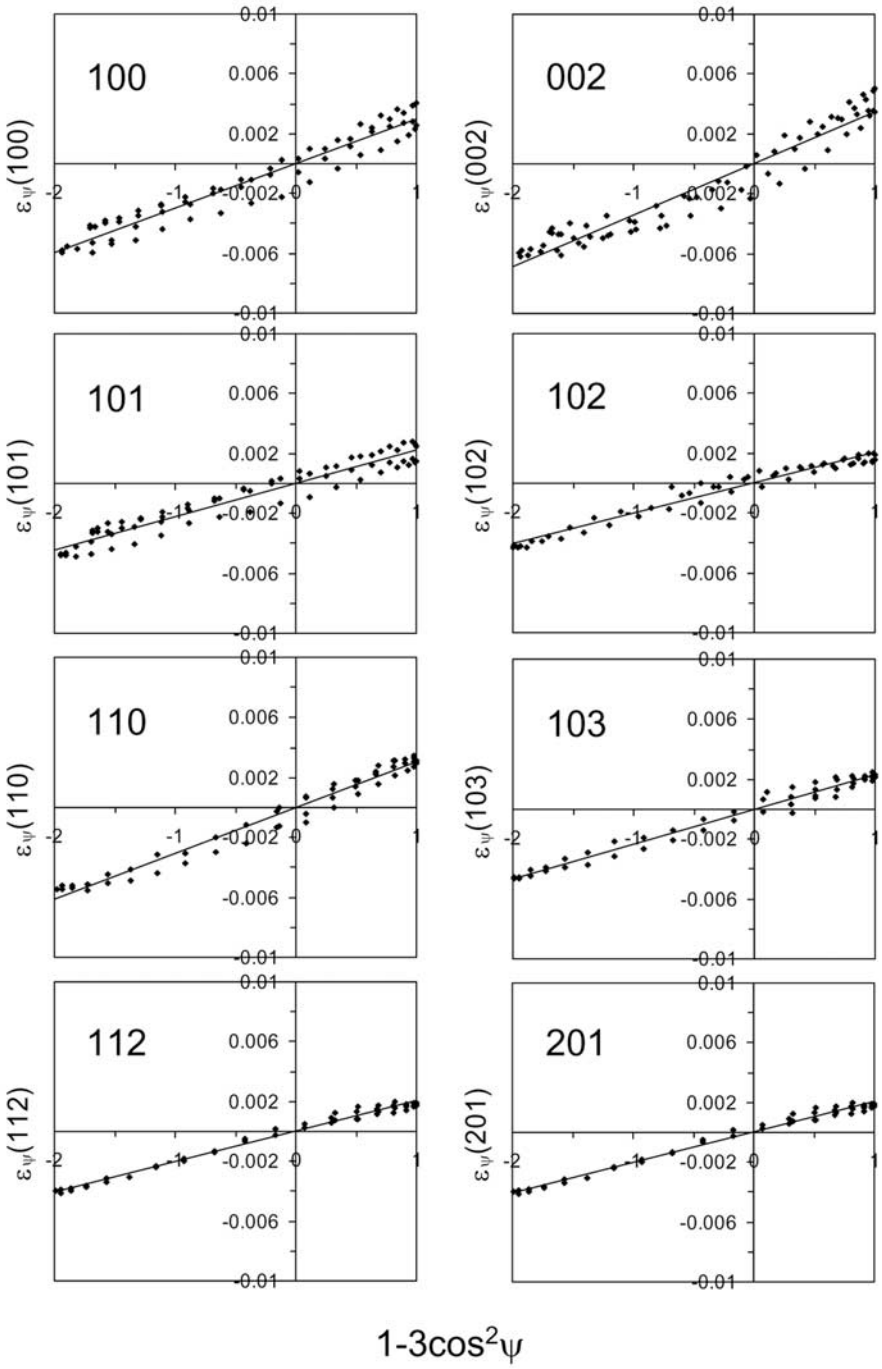

Figure 5. Deviatoric strain as a function of $1-3\cos^2\psi$. The slope of these plots gave the value for $Q(hkl)$.

[18] Figure 7 was calculated on the basis of isostress analysis. As pointed out in the previous RXD-elasticity study, the strain anisotropy may indicate stress variation due to preferred slip systems [*Mao et al.*, 1998] which was found to be the case in an analog system, hcp Co, when results from RXD-elasticity analysis on a polycrystalline Co sample were compared to single-crystal IXS measurements [*Antonangeli et al.*, 2004a; *Merkel et al.*, 2006]. Clearly further analysis on the possible role of strength anisotropy for hcp Fe (see section 4) is necessary.

3.3. RXD-LPO Analysis

[19] A more accurate determination of the elastic parameters can be achieved by adding information from RXD textural analysis and IXS results to correct for the isostress assumption. We analyzed the ranges $\eta = 0°$ to $105°$ and $255°$ to $360°$ where we had complete spectra for all eight hcp Fe *hkl* lines. These angular ranges are sufficient to

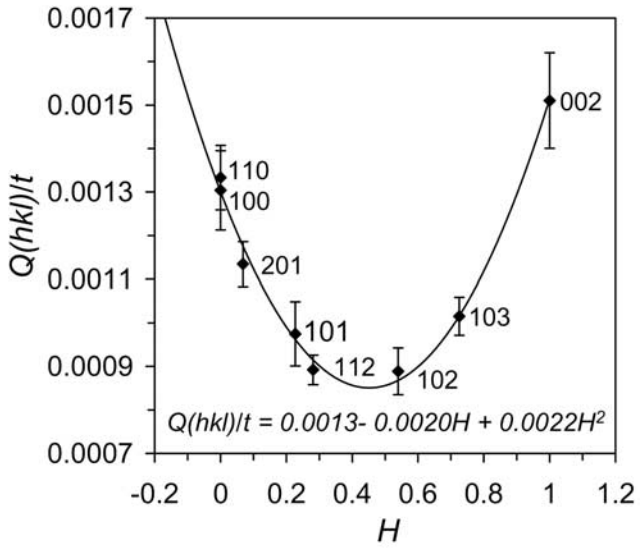

Figure 6. $Q(hkl)/t$ versus H (see equation (8)). The error bars correspond to the 95% confidence intervals for the linear regression fits in the $\varepsilon_\psi(hkl)$ versus $1-3\cos^2\psi$ plots. A parabolic fit provided values for m_1, m_2, and m_3 of 0.0013, −0.0020, and 0.0022 respectively.

analyze the symmetric stress/strain field, which is completely described within a range of 0° (close to perpendicular to compression) and 90° (parallel to compression). Figure 8 shows a stack of 42 such profiles at 5° intervals. The diffraction peaks can be assigned to hcp Fe, with intensity variations due to LPO and systematic 2θ shifts in peak position due to deviatoric stress and elastic anisotropy.

[20] For the textural study, the experimental RXD images were analyzed with the Rietveld method implemented in MAUD (Materials Analysis Using Diffraction) [*Lutterotti et al.*, 1999]. This program calculates integrated diffraction profiles over angular azimuthal slices (for the present analysis we integrated the spectra over 5° intervals). The Rietveld procedure used all the diffraction profiles in the 2θ = 10° to 23° range and taking the DAC tilt into account. First we refined instrumental parameters (detector distance, image center, peak profile, overall intensity), background parameters, unit cell parameters of hcp Fe, and stress (using a simple isotropic triaxial stress model). The bulk modulus and Poisson's ratio for hcp Fe that we used to implement the stress model were derived from the extant literature [*Mao et al.*, 1998; *Stixrude and Cohen*, 1995]. Once a good fit between the calculated and the measured average spectrum was achieved, the texture mode was activated to perform the quantitative LPO analysis, converging after a few cycles. Axial symmetry was imposed. The texture refinement in MAUD relies on the discrete tomographic method WIMV (Williams-Imhof-Matthies-Vinel) [*Matthies and Vinel*, 1982] but allows for arbitrary pole figure coverage. For the resolution of the orientation distribution function (ODF), 20° was used.

[21] At the end of the iterations, the ODF was exported from MAUD and further processed in the code BEARTEX [*Wenk et al.*, 1998] to smooth the ODF and eliminate stochastic effects and to calculate pole figures and inverse pole figures. Orientation densities are expressed as multiples of a random distribution (MRD). Thus an aggregate with no LPO has a probability density of one for all orientations. If preferred orientation is present, some orientations have higher probabilities and others lower probabilities. For axially symmetric textures inverse pole figures are the most informative LPO representation. They give the orientation density of symmetry axes (compression direction) relative to crystal coordinates. The inverse pole figure (Figure 9) shows a maximum of 1.9 MRD at 0001, consistent with an alignment of c axes parallel to the compression direction. This pattern is similar to that observed in previous studies [*Merkel et al.*, 2000; *Wenk et al.*, 2000] but the LPO is much weaker, even for similar pressures. This underscores the importance of LPO characterization of samples for each experiment, limiting the validity of comparison of results from different experimental studies in which LPO is not determined.

3.4. Inelastic X-Ray Scattering

[22] We conducted nonresonant IXS studies at beam line BL35XU of SPring-8 in Japan [*Baron et al.*, 2000] on the same hcp Fe sample at 52 GPa and measured phonon energy as a function of momentum transfer. We carried out two sets of measurements. The medium resolution measurements were taken using the Si (8 8 8) reflection with 6 meV resolution in backscattering mode similar to previous IXS studies on Fe [*Antonangeli et al.*, 2004b; *Fiquet et al.*, 2001]. The high-resolution measurements were taken using the Si (11 11 11) reflection with 1.5 meV resolution. Four spherical analyzer crystals are mounted on the 10 m arm in vacuum, allowing concurrent measurement of four different momentum transfers. This is a very photon intensive experiment, which is made more difficult by the polycrystalline nature of the sample. Each set of four momentum transfers took approximately 12 h at medium resolution and up to 48 h at high resolution to achieve enough counting statistics to resolve the longitudinal phonon of Fe with reasonably small errors. Several sets of data were necessary to constrain the dispersion curve for a particular ψ. The measured energy transfer is scanned by changing the monochromator temperature (with mK precision) over a range of a few degrees which changes its lattice constant due to thermal expansion, and hence the energy of the reflected X rays.

[23] The experimental spectra were fit using Voigt profiles (Figure 10) to give a series of E versus q values that map out the dispersion curve (Figure 11). To estimate V_P, the following fit to a sine dispersion law was used [*Fiquet et al.*, 2001]:

$$E(\mathrm{meV}) = 4.192 \times 10^{-7} V_{P0}\left(\mathrm{kms}^{-1}\right) q_{\max}\left(\mathrm{nm}^{-1}\right) \sin\frac{\pi}{2}\frac{q}{q_{\max}} \tag{26}$$

Table 1. Elastic Parameters for hcp Fe at 52 GPa and 300K Calculated Using RXD-Elasticity and IXS + EOS Method

	RXD-Elasticity (GPa)	IXS + EOS (GPa)
C_{11}	576	599(33)
C_{12}	307	403(20)
C_{13}	324	318(22)
C_{33}	539	650(45)
C_{44}	237	187(40)

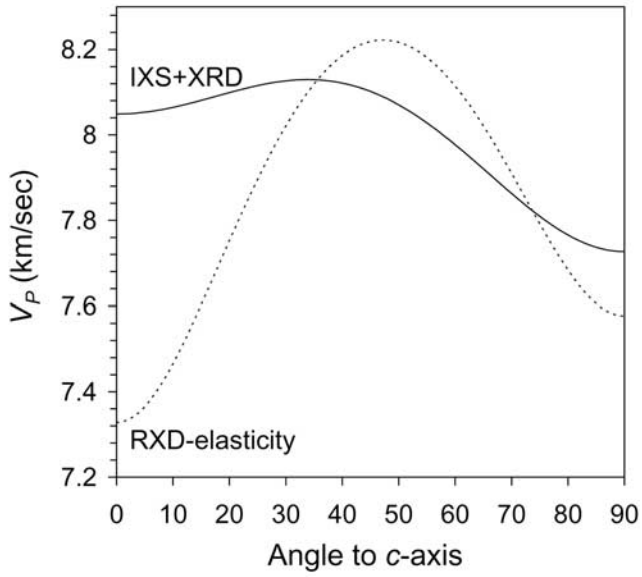

Figure 7. Compressional velocity (V_P) as a function of crystallographic orientation calculated from single crystal elastic tensor determined from RXD-elasticity analysis (dotted line) and from integrated IXS+EOS analysis (solid line).

The results for different ψ at both high and medium resolution are shown in Figure 12 and Table 2 but still have to be corrected for the effects of nonhydrostaticity and LPO.

[24] The use of an X-ray transparent gasket like Be allows complete ψ access in the radial direction compared to previous experiments [*Antonangeli et al.*, 2004b; *Fiquet et al.*, 2001] which used Re gaskets and thus were limited in angular range by what can be accessed axially. Earlier, *Fiquet et al.* [2001] reported results for $\psi = 90°$ only (equivalent to the *a* axis in samples with strong preferred orientation); more recently, *Antonangeli et al.* [2004b] reported results for $\psi = 90°$ and 50°, and found that the body diagonal was faster than the *a* axis. This helps narrow down the possible shapes for the elastic anisotropy, but without knowledge of ψ near 0° (i.e., velocity in the *c axis*) one cannot differentiate between a sigmoidal, bell shape, or more complicated anisotropy. Also, since the samples are not under hydrostatic conditions, there is an error associated with the difference in stress for $\psi = 90°$ and 50° which must be corrected for, but was not addressed by *Antonangeli et al.* [2004b].

3.5. Nuclear Resonance Inelastic X-Ray Scattering

[25] For the NRIXS measurement, an isotopically enriched ^{57}Fe sample was loaded into a 200 μm diameter hole in a Be gasket and compressed between flat diamonds with 400 μm culets. He was loaded as a pressure-transmitting medium, and ruby was added for pressure calibration [*Mao et al.*, 1978; *Zha et al.*, 2000]. A panoramic DAC with large (150°) side openings was used, because the NRIXS signal was collected through the gasket [*Mao et al.*, 2001].

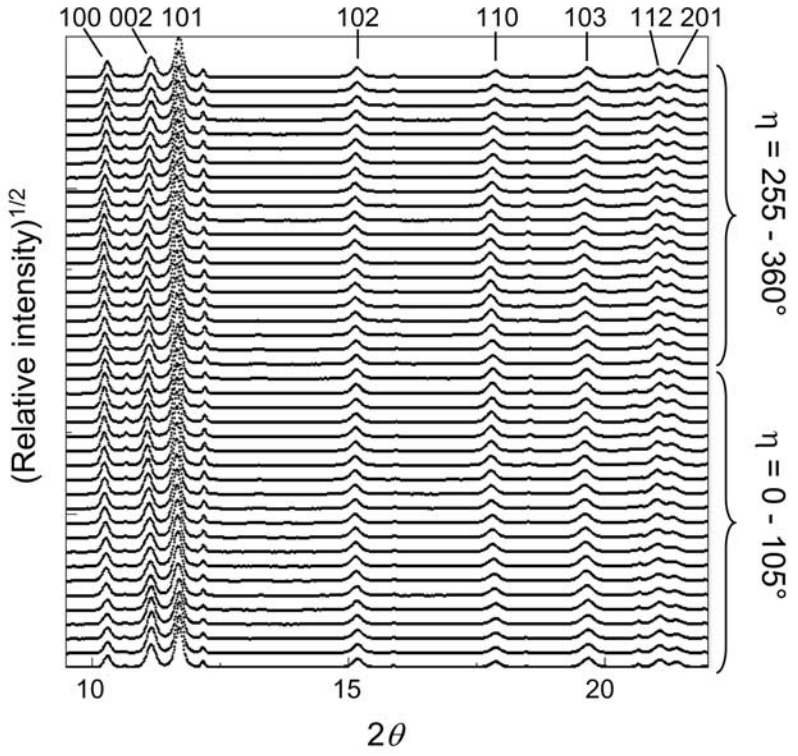

Figure 8. Stack of 42 diffraction profiles for different azimuth angle (η) slices (5° intervals) for hcp Fe at 52 GPa. The weak diffraction peaks between 100 and 002 and to the right of the 101 reflections are from Be.

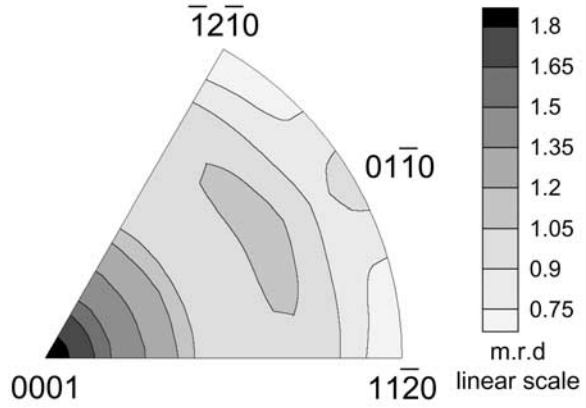

Figure 9. Inverse pole figure of the compression direction for hcp Fe phase at 52 GPa. Orientation densities are expressed in multiples of a random distribution (MRD).

[26] We carried out the NRIXS experiments at beam line 3-ID of the APS, ANL. The phonon excitation spectra took approximately 12 h to collect and was converted to give the Fe phonon DOS (Figure 13) [*Sturhahn*, 2000; *Sturhahn et al.*, 1995]. Debye-like behavior at low phonon energy is assumed, and from a parabolic fit of the low-energy portion the DOS ($g(E)$), V_D can be extracted [*Hu et al.*, 2003]:

$$g(E) = \chi \frac{E^2}{2\pi^2 \hbar^3 n V_D^3} \tag{27}$$

where χ is the ratio of the mass of the nuclear resonant isotope to the average atomic mass (in the case of a pure isotopically enriched ^{57}Fe sample, χ is unity) and n is the density of atoms. For our sample at 50 GPa, we found V_D was 4.53 km s^{-1}. The NRIXS measurement provides an orientationally averaged velocity due to the incoherent nature of the nuclear resonant absorption process. However, to further ensure an orientationally averaged velocity, we sought to maintain a randomly oriented polycrystalline sample through the use of He as a pressure-transmitting medium which provided hydrostatic conditions to suppress development of a preferred orientation.

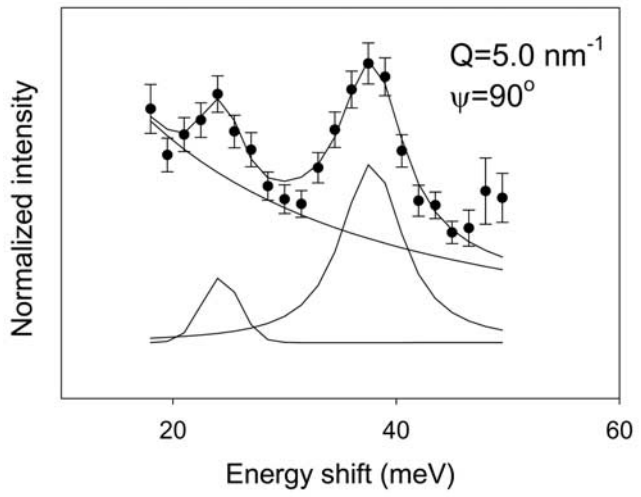

Figure 10. Representative IXS scan at 52 GPa. The Fe longitudinal acoustic peak (left) and diamond peak (right) are clearly visible.

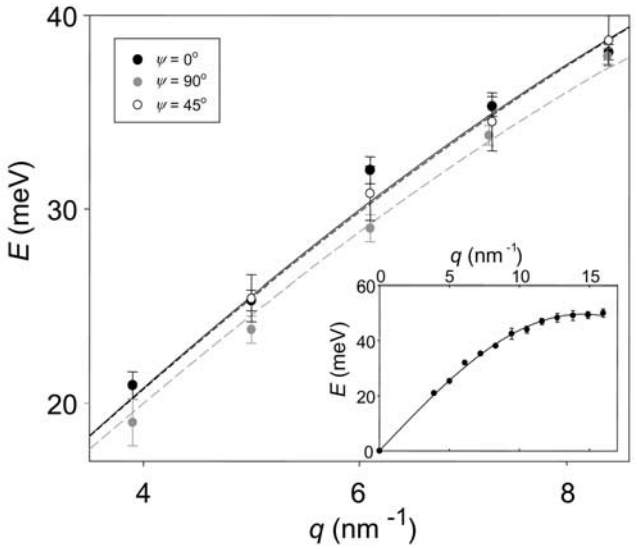

Figure 11. E versus q curves for medium resolution data for three orientations of the DAC (ψ = 0°, 45°, and 90°). Inset shows the sine wave dispersion law fit for the ψ = 0° data set.

4. Data Analysis and Discussion

[27] The elastic parameters of importance for hcp Fe include the five C_{ij} (C_{11}, C_{33}, C_{12}, C_{13}, and C_{44}), bulk (K_S) and shear moduli (G), aggregate V_P and V_S, and single-crystal V_P, V_{S1}, and V_{S2} as a function of orientation. Determination of five independent parameters is sufficient

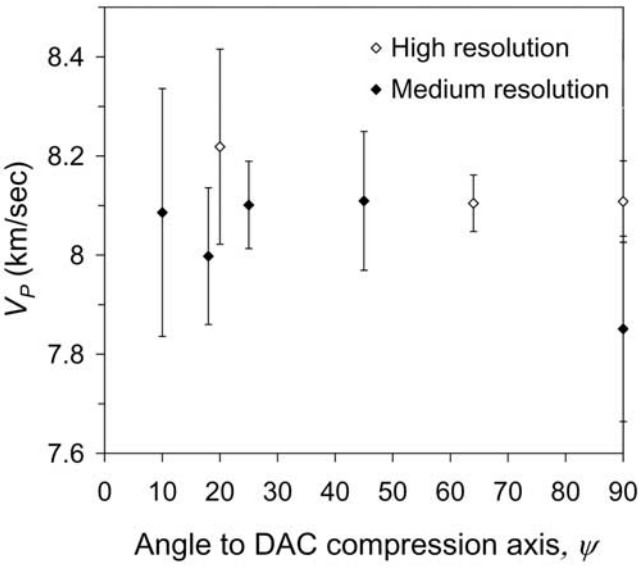

Figure 12. Compressional velocity with 1σ uncertainties as a function of angle to c axis (ψ) for high and medium resolution. The a axis corresponds to ψ = 0°, and the c axis corresponds to ψ = 90°.

Table 2. Compressional Velocity Measurements From IXS at High (1.5 meV) and Medium (6 meV) Resolution

ψ (°)	$V_{P0}(\psi)$(km s^{-1})	$\pm\sigma$ (km s^{-1})
	High Resolution	
20	8.260	0.197
64	8.094	0.057
90	8.083	0.082
	Medium Resolution	
10	8.134	0.250
18	8.041	0.138
25	8.138	0.088
50	8.122	0.140
90	7.826	0.187

for defining the rest of the parameters. Earlier DAC work was limited to determination of the isothermal bulk modulus (K_T) from fitting the EOS data obtained from hydrostatic XRD. Here we developed a procedure to accurately determine the elastic parameters based on an optimized integration of methods.

4.1. Aggregate V_P

[28] Although the aggregate V_P for hcp Fe can also be determined from an RXD-elasticity + EOS combination [*Mao et al.*, 1998], or an NRIXS + EOS combination [*Mao et al.*, 2001], the most direct and accurate measurements potentially come from IXS, although the measurements of aggregate V_P may carry uncertainties caused by differential stress and the LPO in the sample. As a result, the previous axial IXS measurement of aggregate V_P ($\psi = 90°$) [*Fiquet et al.*, 2001] is 3–5% too low in comparison to the V_P measured at $\psi = 50°$ [*Antonangeli et al.*, 2004b], indicating the combined effects of differential stress and LPO as a function of ψ.

[29] The preferred orientation is weak in the present experiment, and therefore errors caused by LPO are minimal. With RXD, we have determined the stress as a function of ψ. The pressure (stress) dependence of V_P is $\partial V_P/\partial P$ = 0.033 km s^{-1} GPa [*Mao et al.*, 2001]. We calculated corrected values of $V_P(\psi)$ from the measured V_{P0} for P = 52 GPa at the 'magic angle' (i.e., when 3 $\cos^2\psi = 1$, so ψ = 54.74°).

$$V_P(\psi) = V_{P0} + 0.033\left(1 - 3\cos^2\psi\right)t/3\left(\text{km s}^{-1}\right) \qquad (28)$$

We took a weighted average of $V_P(\psi)$ over all ψ. The determined aggregate V_P at 52 GPa is thus 8.094 ± 0.07 km s^{-1}.

4.2. Aggregate V_S

[30] Aggregate V_S can also be determined from either an RXD-elasticity + EOS combination [*Mao et al.*, 1998] or a NRIXS + EOS combination [*Mao et al.*, 2001], with the latter providing the better constraint on shear properties, since V_D depends heavily on V_S. A small correction for pressure was applied to the V_D determined at 50 GPa by NRIXS to give V_D = 4.56 ± 0.04 km s^{-1} at 52 GPa. With the aggregate V_P from section 4.1 and equation (3), we obtain a determination of V_S = 4.07 ± 0.04 km s^{-1}.

4.3. K_S and G

[31] Previous values of K_S from XRD include errors introduced from the EOS fit of the isothermal bulk modulus, K_T and the subsequent conversion of K_T to K_S. Only P and ρ are measured; the K_T obtained from derivative of an empirical curve depends upon the form of EOS and assumptions of higher-order truncations. The $K_S = K_T(1 + \alpha\gamma T)$ conversion uncertainty depends upon assumptions for the values of α and γ, and while negligible at ambient T it would become significant above 1000 K.

[32] Our calculation of the elastic tensor is consistent with the adiabatic formulation. In the present case we used the V_P and V_S from IXS and NRIXS and ρ from the EOS, and the K_S = 436 ± 9 GPa and G = 166 ± 3 GPa were calculated from equation (1), thus avoiding the amplified errors of derivatives and the uncertainty of the K_T to K_S conversion. For comparison, the elastic tensor calculated from static lattice strains is isothermal.

4.4. C_{11} and C_{33}

[33] C_{11} and C_{33} can be most directly calculated from equations (24) and (25). The observed values are $V_P(0°)_{\text{obs}}$ = 8.084 ± 0.11 km s^{-1} and $V_P(90°)_{\text{obs}}$ = 8.013 ± 0.07 km s^{-1}. They are both slightly smaller than the aggregate V_P of 8.094 ± 0.08 km s^{-1} from section 4.2 but within the experimental uncertainty. Since our sample had only limited LPO, we need to make an extrapolation to 100% orientation (i.e., c axes of all hcp Fe crystals parallel to the DAC axis). From our RXD-LPO analysis we made the assumption that the LPO in the sample was equivalent to a sample with 22% of the crystal grains oriented with their c axis aligned to the compression axis and the remaining 78% of the grains randomly oriented. The corrected values were $V_P(0°)$ = 8.049 ± 0.30 km s^{-1} and $V_P(90°)$ = 7.727 ± 0.24 km s^{-1}. Substituting these results into equations (24) and (25), we get C_{11} = 599 ± 33 GPa and C_{33} = 650 ± 45 GPa. Only random errors are propagated; additional uncertainties due to the above assumption about correcting for the LPO are not included.

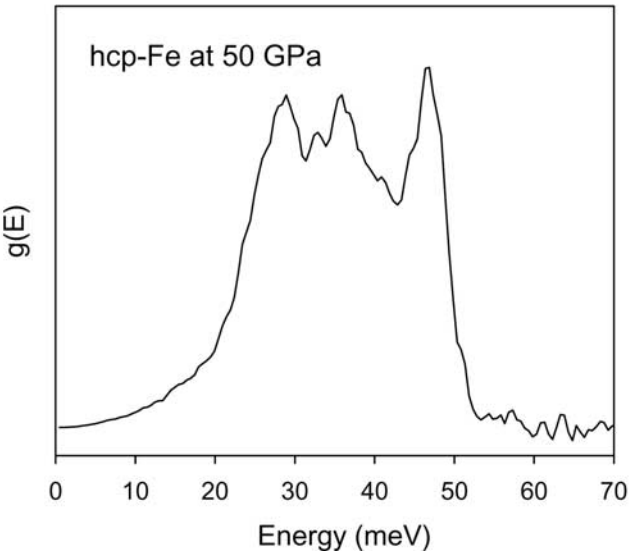

Figure 13. Phonon DOS for Fe at 50 GPa in He medium.

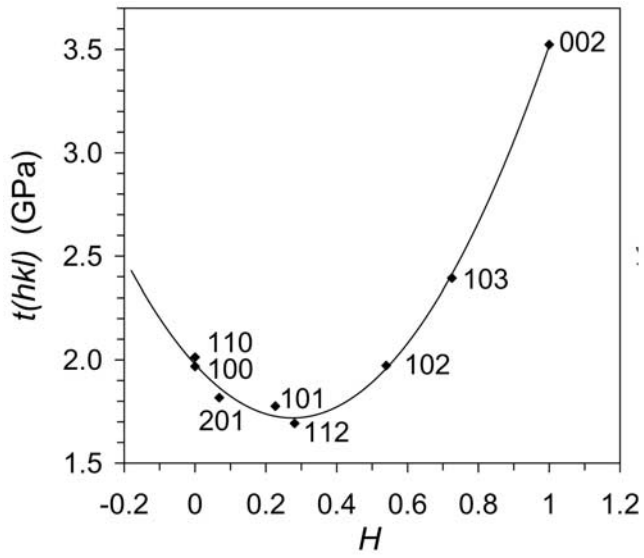

Figure 14. The $t(hkl)$ versus H (see equation (8)). A parabolic fit provided values for n_1, n_2, and n_3 of 1.979, −1.887, and 3.426 respectively.

4.5. C_{12} and C_{13}

[34] The compressibilities of a and c are related to S_{ij} by equations (13) and (14) which can be rewritten in terms of C_{ij} as

$$\chi_a = S_{11} + S_{12} + S_{13} = (C_{33} - C_{13})/C^2 \tag{29}$$

$$\chi_c = S_{33} + 2S_{13} = (C_{11} + C_{12} - 2C_{13})/C^2 \tag{30}$$

$$C^2 = C_{33}(C_{11} + C_{12}) - 2C_{13}^2 \tag{31}$$

Rearrangement of terms yields

$$C_{13} = (1 - C_{33}\chi_c)/2\chi_a \tag{32}$$

$$C_{12} = \left(C_{33} - C_{13} - C_{11}C_{33}\chi_a + 2C_{13}^2\chi_a\right)/C_{33}\chi_a \tag{33}$$

On the basis of the XRD determination [*Jephcoat et al.*, 1986] of the axial ratio, $c/a = 1.606 - 0.00012P$ (GPa) and the Reuss relation $2\chi_a + \chi_c = 1/K_S$, the compressibilities of a and c can be calculated from:

$$\chi_a = \left[1/K_S - 0.000075\left(\mathrm{GPa}^{-1}\right)\right]/3 \tag{34}$$

$$\chi_c = \left[1/K_S + 0.00015\left(\mathrm{GPa}^{-1}\right)\right]/3 \tag{35}$$

Using the already determined values of C_{11}, and C_{33}, we now get $C_{13} = 318 \pm 22$ GPa and $C_{12} = 403 \pm 20$ GPa from equations (34) and (35).

4.6. C_{44}

[35] With C_{11}, C_{33}, C_{12}, and C_{13} determined, equation (21) can be expressed as a function of C_{44}, i.e., $V_P = f(\psi, C_{44})$. The aggregate V_P is an average of ψ from 0 to 90°.

$$V_P = \frac{\int_0^{90} V_P(\psi, C_{44})d\psi}{\int_0^{90} d\psi} = 8.094\,\mathrm{km\ s^{-1}} \tag{36}$$

Solving equation (36) yields $C_{44} = 187 \pm 40$ GPa. This value is considerably lower than the previous result predicted from RXD-elasticity (257 GPa) [*Mao et al.*, 1998], slightly higher than the value for C_{44} inferred from Raman spectroscopy results (~180 GPa) [*Merkel et al.*, 2000], and slightly lower than recent theoretical results (217 GPa) [*Vocadlo et al.*, 2003]. The values for the C_{ij} of hcp Fe at 52 GPa determined by the IXS + EOS method are given in Table 2.

4.7. Velocity Anisotropy and Strength Anisotropy

[36] The velocity anisotropy of hcp Fe at 52 GPa was calculated from equations (21)–(23) and is plotted in Figure 7. We found that the velocity anisotropy of hcp Fe at 52 GPa had a maximum at 34° and a shape that is less bell-shaped and more sigmoidal compared with the RXD-elasticity analysis with a faster c compared to a axis. Also the magnitude of the anisotropy was much smaller (approximately 5% difference between the maximum and minimum V_P compared to 11.5% from RXD-elasticity). The difference between the anisotropy calculated by these two methods is due to the strength anisotropy for different hkl and demonstrates the potential pitfall for assuming constant t in the RXD analysis.

[37] The dependence of t on the hkl can be determined by using the new values for S_{ij} to calculate new m_1, m_2, and m_3 values for the right hand side of equation (7). This was then equated to $Q(hkl)/t(hkl)$ for each data point corresponding to a H value for a hcp Fe reflection. $t(hkl)$ was determined from the measured $Q(hkl)$ in Figure 6 and then fit to a parabolic function

$$t(hkl) = n_1 + n_2H + n_3H^2 \tag{37}$$

and is plotted in Figure 14.

5. Conclusions

[38] This study presents an approach for the complete experimental characterization of the elasticity of hcp Fe under pressure. We present a suite of synchrotron techniques that are available for studying elasticity and LPO at high pressure as well as a methodology for integrating the results in order to produce accurate well-constrained data. A unique advantage of this experimental data set is that multiple measurements were conducted on the same sample, allowing for integration of results with consistent conditions. We found that the velocity anisotropy of hcp Fe at 52 GPa has a maximum near the body diagonal between the a and c axes, but with a shape closer than sigmoidal than that from the RXD-elasticity calculations (Figure 14). Incorporation of RXD-LPO with IXS directional phonon and EOS results allow for a more accurate determination of

the elastic parameters. This type of analysis needs to be extended to higher P and high T, but until static measurements can be made at inner core P-T conditions, verification of calculations over the region where experiment and theory overlap is of critical importance.

[39] Although the uncertainties for the present results are still large, and extended extrapolation in both pressure and temperature are required to reach the core conditions, we can draw tentative implications about inner core anisotropy. The maximum velocity anisotropy of 5%, would require significant alignment of the hcp Fe crystals in order to account for the observed inner core anisotropy unless the velocity anisotropy increases at high pressures and temperatures. If the shape of anisotropy remains the same to inner core conditions, one can expect that the hcp Fe crystals would be aligned with their c axis in the polar direction and a axis in the equatorial direction.

[40] This study also highlights the current experimental limitations for core elasticity studies and presents a strategy for future studies of hcp Fe elasticity. With an integrated approach, existing techniques could yield much more accurate elasticity data for comparison with theories and seismological observations. For instance, a large source of uncertainty of the present results comes from the sample being neither hydrostatic nor having strong LPO. For accurate determination of the full elasticity at a given P-T point, it would be optimal, for example, to prepare two separate experiments on ^{57}Fe-enriched samples in Be gaskets in panoramic DACs: one with a He pressure medium to provide a hydrostatic environment, and the other without a pressure medium to provide axial stress conditions in order to maximize the preferred orientation. RXD can be used to confirm the lack of lattice preferred orientation (LPO) in the hydrostatic DAC sample and to determine the degree of LPO in the axially stressed DAC sample. IXS measurements on the hydrostatic sample provide the most robust determination of aggregate V_P, which when combined with NRIXS measurements provide accurate determination of aggregate V_S; K_S, and G, can then be calculated directly from aggregate V_P and V_S. IXS measurements on the axially stressed sample at $\psi = 0°$ and 90° with corrections for the degree of LPO and stress differences will constrain C_{33} and C_{11} respectively. XRD measurements on a hydrostatic DAC sample then provide χ_a and χ_c which can be used to calculate C_{12} and C_{13} (equations (32) and (33)). The remaining elastic tensor component C_{44} can then be determined from the known values of the other tensor elements. Using this strategy, IXS measurements from the axially stressed sample at ψ angles besides 0° and 90° are not required but will be helpful for verification. Also, the RXD analysis of anisotropic lattice strain will not be used for C_{ij} determination but instead provides measurement of anisotropic lattice strength. We estimate that with the combined hydrostatic and maximum LPO approach, the propagated errors in C_{ij} could be reduced by a factor of four compared to the present results, and could provide stringent constraints on ab initio calculations and seismic models. Simultaneous high P-T with laser-heated DAC have been developed for NRIXS and RXD, and can conceivably be integrated with IXS. With the continued advances in synchrotron capabilities and high-pressure technology, the integrated measurements may ultimately be extended to the core conditions.

[41] **Acknowledgments.** The authors would like to thank F. M. Richter, B. A. Buffet, W. A. Bassett, and two anonymous reviewers for helpful comments on the manuscript. W. Mao is supported through the Geophysics program at NSF (EAR-0738873). H. R. Wenk acknowledges support from NSF (EAR-0337006) and the Carnegie DOE Alliance Center (CDAC). The HPCAT facility is supported by DOE-BES, DOE-NNSA (CDAC), NSF (EAR-0337006 and 0409321), DOD –TACOM, and the W.M. Keck Foundation. The Advanced Photon Source is supported by the U. S. Department of Energy, Office of Science, Office of Basic Energy Sciences, under contract DE-AC02-06CH11357. Use of BL35XU in SPring-8 was supported by the Japan Synchrotron Radiation Research Institute (JASRI), and the IXS experiments were performed with their approval (proposal 2003A0022-ND3-np and 2003B0693-ND3d-np).

References

Antonangeli, D., et al. (2004a), Elasticity of cobalt at high pressure studied by inelastic X-ray scattering, *Phys. Rev. Lett.*, *93*, 215505, doi:10.1103/PhysRevLett.93.215505.

Antonangeli, D., et al. (2004b), Elastic anisotropy in textured hcp-iron to 112 GPa from sound wave propagation measurements, *Earth Planet. Sci. Lett.*, *225*, 243–251, doi:10.1016/j.epsl.2004.06.004.

Baron, A. Q. R., et al. (2000), An X-ray scattering beamline for studying dynamics, *J. Phys. Chem. Solids*, *61*, 461–465, doi:10.1016/S0022-3697(99)00337-6.

Bassett, W. A., and E. M. Brody (1977), Brillouin scattering: A new way to measure elastic moduli at high pressures, in *High Pressure Research—Applications in Geophysics*, edited by M. Manghnani and S. Akimoto, pp. 519–532, Academic, New York.

Birch, F. (1952), Elasticity and constitution of the Earth's interior, *J. Geophys. Res.*, *57*, 227–286, doi:10.1029/JZ057i002p00227.

Bréger, L., B. Romanowicz, and S. Rousset (2000), New constraints on the structure of the inner core from P′P′, *Geophys. Res. Lett.*, *27*, 2781–2784.

Cao, A., and B. Romanowicz (2004), Hemispherical transition of seismic attenuation at the top of the earth's inner core, *Earth Planet. Sci. Lett.*, *228*, 243–253, doi:10.1016/j.epsl.2004.09.032.

Creager, K. C. (1992), Anisotropy of the inner core from differential travel times of the phases PKP and PKIKP, *Nature*, *356*, 309–314, doi:10.1038/356309a0.

Creager, K. C. (1999), Large-scale variations in inner core anisotropy, *J. Geophys. Res.*, *104*, 23,127–23,139, doi:10.1029/1999JB900162.

Crowhurst, J. C., et al. (2004), Impulsive stimulated light scattering from opaque materials at high pressure, *J. Phys. Condens. Matter*, *16*, S1137–S1142, doi:10.1088/0953-8984/16/14/023.

Dewaele, A., et al. (2006), Quasihydrostatic equation of state of iron above 2 Mbar, *Phys. Rev. Lett.*, *97*, 215504, doi:10.1103/PhysRevLett.97.215504.

Fiquet, G., et al. (2001), Sound velocities in iron to 110 gigapascals, *Science*, *291*, 468–471, doi:10.1126/science.291.5503.468.

Gannarelli, C. M. S., et al. (2005), The axial ratio of hcp iron at the conditions of the Earth's inner core, *Phys. Earth Planet. Inter.*, *152*, 67–77, doi:10.1016/j.pepi.2005.06.003.

Hammersley, A. P. (1997), FIT2D: An introduction and overview, *ESRF Rep. ESRF97HA02T*, Eur. Synchrotron Radiat. Facil., Grenoble, France.

Hemley, R. J., and H. K. Mao (2001), In-situ studies of iron under pressure: New windows on the Earth's core, *Int. Geol. Rev.*, *43*, 1–30.

Hu, M. Y., et al. (2003), Measuring velocity of sound with nuclear resonant inelastic X-ray scattering, *Phys. Rev. B*, *67*, 094304, doi:10.1103/PhysRevB.67.094304.

Ishii, M., and A. Dziewonski (2002), The innermost inner core of the earth: Evidence for a change in anisotropic behavior at the radius of about 300 km, *Proc. Natl. Acad. Sci. U.S.A.*, *99*, 14,026–14,030, doi:10.1073/pnas.172508499.

Jephcoat, A. P., et al. (1986), The static compression of iron to 78 GPa with rare gas solids as pressure-transmitting media, *J. Geophys. Res.*, *91*, 4677–4684, doi:10.1029/JB091iB05p04677.

Laio, A., et al. (2000), Physics of iron at earth's core conditions, *Science*, *287*, 1027–1030, doi:10.1126/science.287.5455.1027.

Lin, J.-F., W. Sturhahn, J. Zhao, G. Shen, H. Mao, and R. J. Hemley (2004), Absolute temperature measurement in a laser-heated diamond anvil cell, *Geophys. Res. Lett.*, *31*, L14611, doi:10.1029/2004GL020599.

Lutterotti, L., et al. (1999), MAUD: A friendly Java program for materials analysis using diffraction, *Inter. Union Crystallogr. Comm. Powder Diffract. Newsl.*, *21*, 14–15.

Ma, Y., et al. (2004), In-situ X-ray diffraction studies of iron to Earth-core conditions, *Phys. Earth Planet. Inter.*, *143–144*, 455–467.

Mao, H. K., et al. (1978), Specific volume measurements of Cu, Mo, Pd, and Ag and calibration of the ruby R_1 fluorescence pressure gauge from 0.06 to 1 Mbar, *J. Appl. Phys.*, *49*, 3276–3283, doi:10.1063/1.325277.

Mao, H. K., et al. (1990), Static compression of iron to 300 GPa and $Fe_{0.8}Ni_{0.2}$ alloy to 260 GPa: Implications for composition of the core, *J. Geophys. Res.*, *95*, 21,737–21,742, doi:10.1029/JB095iB13p21737.

Mao, H. K., et al. (1998), Elasticity and rheology of iron above 220 GPa and the nature of the Earth's inner core, *Nature*, *396*, 741–743, doi:10.1038/25506. (Correction–Elasticity and rheology of iron above 220 GPa and the nature of the Earth's inner core, *Nature*, *399*, 280, doi:10.1038/20472, 1999.).

Mao, H. K., et al. (2001), Phonon density of states of iron up to 153 GPa, *Science*, *292*, 914–916, doi:10.1126/science.1057670.

Matthies, S., and G. W. Vinel (1982), On the reproduction of the orientation distribution function of textured samples from reduced pole figures using the concept of conditional ghost correction, *Phys. Status Solidi B*, *112*, K111–K114, doi:10.1002/pssb.2221120254.

Matthies, S., et al. (2001), Effect of texture on the determination of elasticity of polycrystalline ε-iron from diffraction measurements, *Earth Planet. Sci. Lett.*, *194*, 201–212, doi:10.1016/S0012-821X(01)00547-7.

Merkel, S., et al. (2000), Raman spectroscopy of iron to 152 gigapascals: Implications for Earth's inner core, *Science*, *288*, 1626–1629, doi:10.1126/science.288.5471.1626.

Merkel, S., J. Shu, P. Gillet, H.-K. Mao, and R. J. Hemley (2005), X-ray diffraction study of the single-crystal elastic moduli of ϵ-Fe up to 30 GPa, *J. Geophys. Res.*, *110*, B05201, doi:10.1029/2004JB003197.

Merkel, S., et al. (2006), Lattice preferred orientation and stress in polycrystalline hcp-Co plastically deformed under high pressure, *J. Appl. Phys.*, *100*, 023510, doi:10.1063/1.2214224.

Morelli, A., et al. (1986), Anisotropy of the inner core inferred from PKIKP travel times, *Geophys. Res. Lett.*, *13*, 1545–1548, doi:10.1029/GL013i013p01545.

Murakami, M., et al. (2007), Sound velocity of $MgSiO_3$ perovskite to Mbar pressure, *Earth Planet. Sci. Lett.*, *256*, 47–54, doi:10.1016/j.epsl.2007.01.011.

Musgrave, M. J. P. (1970), *Crystal Acoustics*, Holden-Day, San Francisco, Calif.

Olijnyk, H., and A. P. Jephcoat (2000), Optical zone-centre phonon modes and macroscopic elasticity in hcp metals, *Solid State Commun.*, *115*, 335–339, doi:10.1016/S0038-1098(00)00207-6.

Olijnyk, H., et al. (2001), On optical phonons and elasticity in the hcp transition metals Fe, Ru and Re at high pressure, *Europhys. Lett.*, *53*, 504–510, doi:10.1209/epl/i2001-00181-4.

Romanowicz, B., et al. (2002), On the origin of complexity in PKP travel time data from broadband records, in *Earth's Core: Dynamics, Structure, Rotation*, *Geodyn. Ser.*, vol. 31, edited by V. Dehant and K. Creager, pp. 31–44, AGU, Washington, D. C.

Shearer, P. M. (1994), Constraints on inner core anisotropy from PKP(DF) travel times, *J. Geophys. Res.*, *99*, 19,647–19,659, doi:10.1029/94JB01470.

Singh, A. K., et al. (1998a), Analysis of lattice strains measured under nonhydrostatic pressure, *J. Appl. Phys.*, *83*, 7567–7575, doi:10.1063/1.367872.

Singh, A. K., et al. (1998b), Estimation of single-crystal elastic moduli from polycrystalline X-ray diffraction at high pressure: Applications to FeO and iron, *Phys. Rev. Lett.*, *80*, 2157–2160, doi:10.1103/PhysRevLett.80.2157.

Söderlind, P., et al. (1996), First-principles theory of iron up to Earth-core pressures: Structural, vibrational, and elastic properties, *Phys. Rev. B*, *53*, 14,063–14,072, doi:10.1103/PhysRevB.53.14063.

Song, X., and D. Helmberger (1993), Anisotropy of the Earth's inner core, *Geophys. Res. Lett.*, *20*, 2591–2594, doi:10.1029/93GL02812.

Song, X. D., and D. V. Helmberger (1995), Depth dependence of anisotropy of Earth's inner core, *J. Geophys. Res.*, *100*, 9805–9816, doi:10.1029/95JB00244.

Steinle-Neumann, G., et al. (1999), First-principles elastic constants for the hcp transition metals Fe, Co, and Re at high pressure, *Phys. Rev. B*, *60*, 791–799, doi:10.1103/PhysRevB.60.791.

Steinle-Neumann, G., et al. (2001), Elasticity of iron at the temperature of the Earth's inner core, *Nature*, *413*, 57–60, doi:10.1038/35092536.

Stixrude, L., and R. E. Cohen (1995), High-pressure elasticity of iron and anisotropy of Earth's inner core, *Science*, *267*, 1972–1975, doi:10.1126/science.267.5206.1972.

Stixrude, L., et al. (1997), Composition and temperature of Earth's inner core, *J. Geophys. Res.*, *102*, 24,729–24,739, doi:10.1029/97JB02125.

Sturhahn, W. (2000), CONUSS and PHOENIX: Evaluation of nuclear resonant scattering, *Hyperfine Interact.*, *125*, 149–172, doi:10.1023/A:1012681503686.

Sturhahn, W., et al. (1995), Phonon density of states measured by inelastic nuclear resonant scattering, *Phys. Rev. Lett.*, *74*, 3832–3835, doi:10.1103/PhysRevLett.74.3832.

Sun, X. L., and X. D. Song (2002), PKP travel times at near antipodal distances: Implications for inner core anisotropy and lowermost mantle structure, *Earth Planet. Sci. Lett.*, *199*, 429–445, doi:10.1016/S0012-821X(02)00580-0.

Tromp, J. (1993), Support for anisotropy of the Earth's inner core from free oscillations, *Nature*, *366*, 678–681, doi:10.1038/366678a0.

Vinnik, L., et al. (1994), Anisotropy in the center of the inner core, *Geophys. Res. Lett.*, *21*, 1671–1674, doi:10.1029/94GL01600.

Vocadlo, L., et al. (2000), Ab inito free energy calculations on the polymorphs of iron at core conditions, *Phys. Earth Planet. Inter.*, *117*, 123–137, doi:10.1016/S0031-9201(99)00092-8.

Vocadlo, L., et al. (2003), The properties of iron under core conditions from first principles calculations, *Phys. Earth Planet. Inter.*, *140*, 101–125, doi:10.1016/j.pepi.2003.08.001.

Wenk, H. R., et al. (1998), BEARTEX: A Window-based program system for quantitative texture analysis, *J. Appl. Crystallogr.*, *31*, 262–269, doi:10.1107/S002188989700811X.

Wenk, H.-R., et al. (2000), The plastic deformation of iron at pressures of the Earth's inner core, *Nature*, *405*, 1044–1047, doi:10.1038/35016558.

Wenk, H.-R., et al. (2006), Deformation textures produced in diamond anvil experiments, analysed in radial diffraction geometry, *J. Phys. Condens. Matter*, *18*, S933–S947, doi:10.1088/0953-8984/18/25/S02.

Woodhouse, J. H., et al. (1986), Evidence for inner core anisotropy from free oscillations, *Geophys. Res. Lett.*, *13*, 1549–1552, doi:10.1029/GL013i013p01549.

Zha, C.-S., et al. (1993), Elasticity of hydrogen to 24 GPa from single-crystal Brillouin scattering and synchrotron X-ray diffraction, *Phys. Rev. B*, *48*, 9246–9255, doi:10.1103/PhysRevB.48.9246.

Zha, C.-S., et al. (2000), Elasticity of MgO and a primary pressure scale to 55 GPa, *Proc. Natl. Acad. Sci. U. S. A.*, *97*, 13,494–13,499, doi:10.1073/pnas.240466697.

A. Q. R. Baron, SPring-8, RIKEN, 1-1-1 Kouto, Sayo, Hyogo, 679-5148, Japan.

P. Chow and M. Y. Hu, HPCAT, Advanced Photon Source, Carnegie Institution of Washington, Washington, DC 20015, USA.

D. L. Heinz, Department of Geophysical Sciences, University of Chicago, Chicago, IL 60637, USA.

R. J. Hemley, H.-K. Mao, J. Shu, and V. V. Struzhkin, Geophysical Laboratory, Carnegie Institution of Washington, Washington, DC 20015, USA.

W. L. Mao, Department of Geological and Environmental Sciences and Photon Science, SLAC, Stanford University, Stanford, CA 94305, USA. (wmao@stanford.edu)

W. Sturhahn, XOR, Advanced Photon Source, Argonne National Laboratory, Argonne, IL 60439, USA.

C. E. Tommaseo, Department of Crystallography, University of Göttingen, D-37077, Göttingen, Germany.

S. Tsutsui, SPring-8, JASRI, 1-1-1 Kouto, Sayo, Hyogo, 679-5198, Japan.

H.-R. Wenk, Department of Earth and Planetary Science, University of California, Berkeley, CA 94720, USA.